Electronic Supplementary Information

Ultra-Low-Voltage Ammonia Production in Overall Chloride-Rich Wastewater Electrolysis of HMF/Nitrite Enabled by a Ta-Induced Multi-Heterostructured Nanocluster Catalyst with Enhanced Photothermal Effect

Han Xie, Xu Yao, Xintong Miao, Shenshi Zhou, Han Yan, Liping Ding*, Qi Li*, Yanqing Wang*

Experimental Section

Materials

K_2TaF_7(99.7%), KOH(95%), $NiSO_4 \cdot 6H_2O$(98.5%), NaCl(99.5%), thiourea(99%), sodium citrate dihydrate(99%), 5-Hydroxymethyl-2-furaldehyde(95%)，ethyl alcohol and H_2SO_4(95-98wt%) were purchased from Sigma Aldrich.

Fabrication of the Ni-Ta-S-O catalyst

The preparation process of the Ni-Ta-S-O catalyst is as follows. First, copper foam is placed in absolute ethanol and ultrasonicated for 2 minutes to remove grease and dust from the surface. Next, copper foam is placed in 5 volume% H_2SO_4 solution for 2 minutes to remove the oxide layer from the surface. Last but not least, the copper foam was placed in a solution which contains 0.8g/L K_2TaF_7, 40g/L sodium citrate dihydrate, 30g/L $NiSO_4 \cdot 6H_2O$, 150g/L thiourea, adjust with 5 volume% H_2SO_4 to a pH of about 3. Copper foam was reacted in the above solution at 60℃ for 5 minutes. Each step of the process is washed with deionized water. Finally, the Ni-Ta-S-O catalyst was successfully fabricated on copper foam. The catalyst loading of Ni-Ta-S-O is about 0.189mg/cm^2.

Characterizations

The microscopic topography of the sample was observed using a field emission scanning electron microscope (SEM, Gemini SEM 300). The XRD pattern of the test sample was used with the Rigaku Ultima IV. X-ray photoelectron spectroscopy (XPS, Thermo Scientific K-Alpha) was used to analyze the surface elements of the sample. The transmission electron microscope (TEM) model number is JEOL JEM-2100HR (LaB6). EDS was tested by JEOL JSM-6510. The concentration of the product was measured using

the Shimadzu UV-1900i spectrophotometer from Japan. The HPLC (Agilent Technologies 1260 Infinity) was Used to detect product concentration.

Electrochemical measurements

All electrochemical tests were performed using a CS3104M Cortest workstation. For the three-electrode configuration, Ni-Ta-S-O/CF or Ni-S/CF served as the working electrode, with a Pt counter electrode and an Hg/HgO reference electrode. The anodic compartment was filled with an electrolyte containing 1 M KOH, 0.6 M NaCl, and 0.1 M HMF, simulating a chloride-rich wastewater stream for biomass valorization. The cathodic compartment contained 1 M KOH, 0.6 M NaCl, and 1 M KNO_2, representing a high-strength nitrite-laden industrial effluent. In the two-electrode system, Ni–Ta–S–O/CF was used as both anode and cathode in a unified electrolyte consisting of 1 M KOH, 1 M KNO_2, 0.6 M NaCl, and 0.1 M HMF, which mimics a co-electrolysis scenario for treating complex wastewater. A Xe lamp was employed to provide simulated solar irradiation with an ntensity approximating sunlight.

The data obtained from the test are converted to relative to the RHE potential by the following formula: $E_{RHE} = E_{Hg/HgO} + 0.059pH + 0.098V$. LSV curves were measured at 5mV/s, the Tafel slopes were measured at 1mV/s and the LPR curves were measured at 0.167mV/s. All electrochemical test data were corrected with 90% IR compensation.

Supplementary Methods

1. Calculating electrochemically active surface area (*ECSA*)

The electric double-layer capacitance C_{dl} of the electrode is calculated by the formula $C_{dl} = J_c/V$. Of these, J_c is obtained by CV curves which in the range of non-Faradic current.

As can be seen from **Fig. 3d, S9f and S10e**, the C_{dl} for different contents of K_2TaF_7 is 3.98mF, 6.97mF, 9.65mF, 8.49mF, 4.22mF, respectively, and the corresponding *ECSA* calculated according to $ECSA = C_{dl}/Cs$ (Cs is usually 0.04 mF/cm^2) is 99.5cm^2, 174.25cm^2, 241.25cm^2, 212.25cm^2, 105.5cm^2, respectively. The C_{dl} value of Ni-Ta-S-O under different reaction time 2min, 5min, 10min and 20min is about 4.11mF, 9.65mF, 9.15mF, 9.22mF, respectively, and the corresponding *ECSA* is 102.75cm^2, 241.25cm^2, 228.75cm^2, 230.5cm^2, respectively. The C_{dl} value of Cu foam, Ni-S and Ni-Ta-S-O is 1.12mF, 3.98mF and 9.65mF, and the *ESCA* of Cu foam, Ni-S and Ni-Ta-S-O is 28cm^2, 99.5cm^2, 241.25cm^2, respectively.

2. Calculating of NH_3 yeild

The NH_3 concentration in the electrolyte was determined by indolyl blue method. Dilute the electrolyte in the appropriate ratio so that the test results fall within the standard curve. The obtained sample was diluted to 4 ml, and three chromogens 4mL of 1M NaOH solution (containing 5% CH_6O_3 and 5% $C_6H_5Na_3O_7{\cdot}2H_2O$), 2mL of 0.05M NaClO solution, and 0.4mL of a mixed solution (dissolve 1 g $Na_2Fe(CN)_5NO{\cdot}2H_2O$ in 100 mL of ultrapure water) were added to it, mixed thoroughly, and left in the dark for 2 hours, then the absorbance at 655 nm is measured by ultraviolet spectrophotometer.

According to the linear relationship between absorbance and concentration gradient, different concentrations of NH_4Cl solution were tested, and the standard curve of NH_4^+ was obtained by fitting the test results shown in our as-reported article (Advanced energy materials, 2024, 14, 2402301)

NH_4^+ faradic efficiency was calculated by:

$$FE_{NH4+}(\%) = {}^{V * c_{NH4+}}/_{A * t}$$

NH_4^+ yield rates is calculated by:

$$NH_4^+\ yeild(\mu g h^{-1} cm^{-2}) = {}^{6 * F * c_{NH4+} * V}/_{M_{NH4+} * Q} * 100\%$$

Where V(mL) is the volume of the electrolyte, c_{NH4+}(μg/mL) is the measured NH_4^+ concentration, A(cm^2) is the facing area of working electrode, t(h) is the reduction time, F is the Faraday constant (96500C·mol^{-1}), M_{NH4+} is the relative molecular mass of NH_4^+, Q is the amount of charge consumed.

3. Calculating of energy saving rate

Calculating the energy expended to produce 1 mol of NH_3 at the same potential by following formula:

$$W = U * I * t$$

$$t = 1mol/NH_4^+\ yeild$$

U(V) is the potential vs Hg/HgO, I(A·cm^{-2}) is the current density, t(h) is the time it takes to produce 1 mol of NH_3, and the $NH_4^+\ yeild$ (μmol·h^{-1}·cm^{-2}) was calculated before.

4. Calculating of HMF Oxidation products

The main oxidation products of HMF are FDCA、HMFCA、FFA. The concentration

of FDCA and HMF was calculated using a standard curve obtained from HPLC testing[29].

Calculating of the HMF conversion:

$$HMF\ conversion = {}^{n_{(HMF\ consumption)}}\Big/_{n_{(before)}} * 100\%$$

Calculating of the FDCA selectively:

$$FDCA\ selectively = {}^{n_{(FDCA)}}\Big/_{n_{(HMF\ con.)}} * 100\%$$

FDCA faradic efficiency was calculated by:

$$FE_{(FDCA)}(\%) = {}^{Z * e * N_A * n_{(FDCA)}}\Big/_{Q} * 100\%$$

Z is the number of electrons transferred in the reaction, while the product is FDCA, Z = 6, e is Elementary charge ($1.6*10^{-19}$C), N_A is Avogadro's constant ($6.02*10^{23}$ mol^{-1}), $n_{(HMF\ consumption)}$ and $n_{(FDCA)}$ was calculated before, and the Q is the amount of charge consumed.

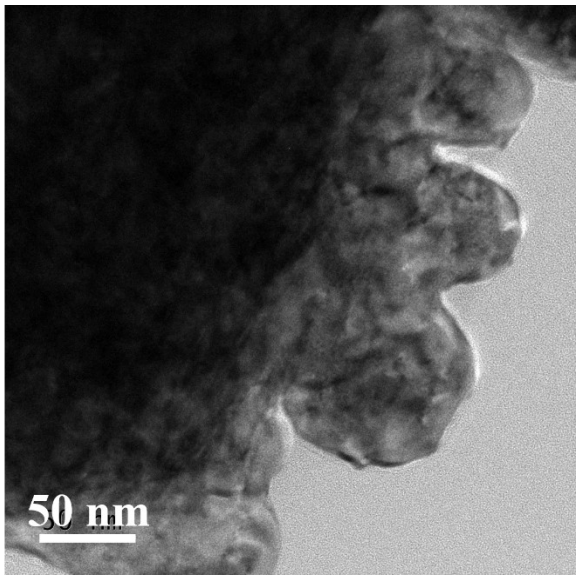

Fig. S1 High resolution TEM image of Ni-Ta-S-O catalytic layer

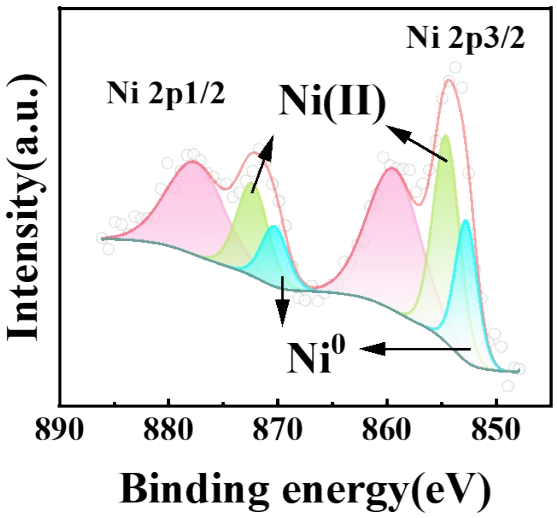

Fig. S2 The XPS fine spectra of Ni element of Ni-S catalytic layer

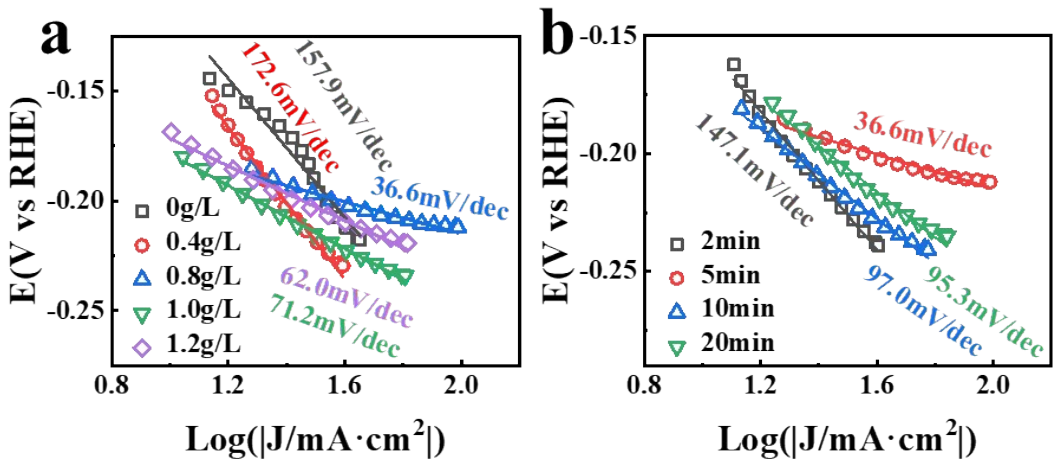

Figure S3 The influence of different K_2TaF_7 concentration(a) and reaction time(b) on NO2RR tafel performance of Ni-Ta-S-O catalyst.

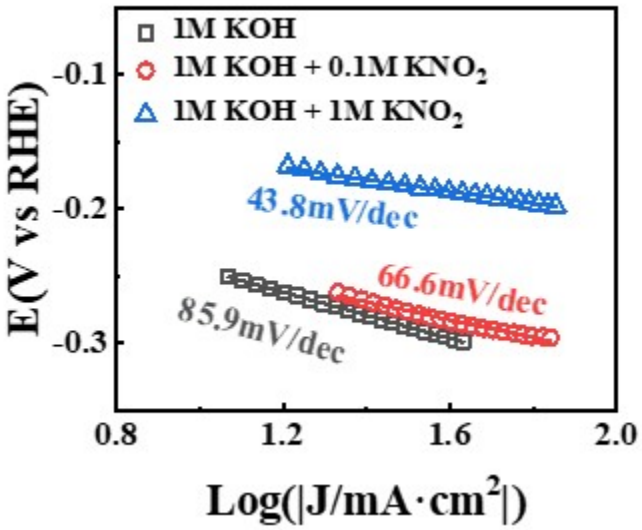

Figure S4 The Tafel performance of Ni-Ta-S-O catalyst for HER and NO2RR in varied electrolyte.

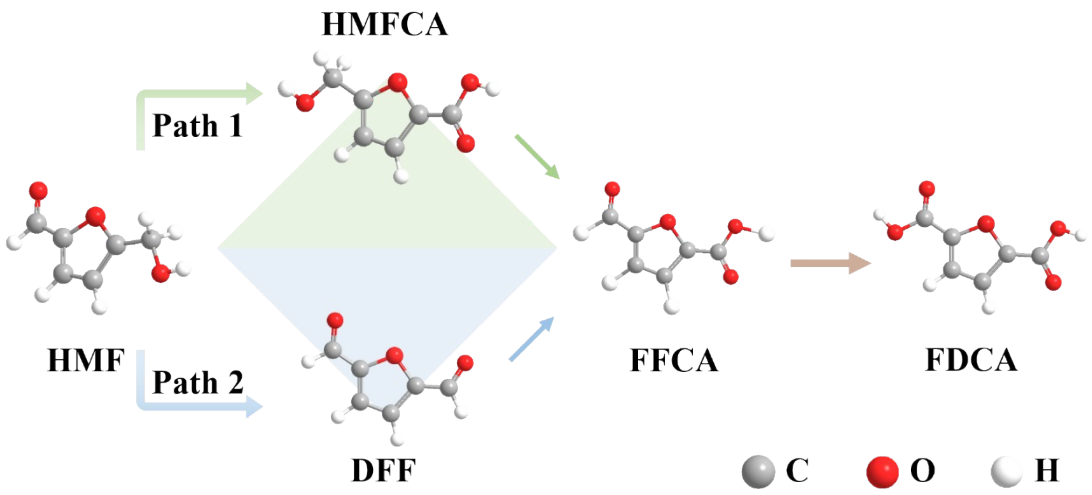

Scheme S1 The possible pathways for 5-Hydroxymethyl-2-furaldehyde oxidization reaction (HMFOR)

Table S1 Comparison of electrochemical polarization resistance R_p value of different catalysts under 0.55V(vs Hg/HgO)

catalyst	$R_p(\Omega \cdot cm^2)$
CF	13.59
Ni-S	4.15
Ni-Ta-S-O	0.85

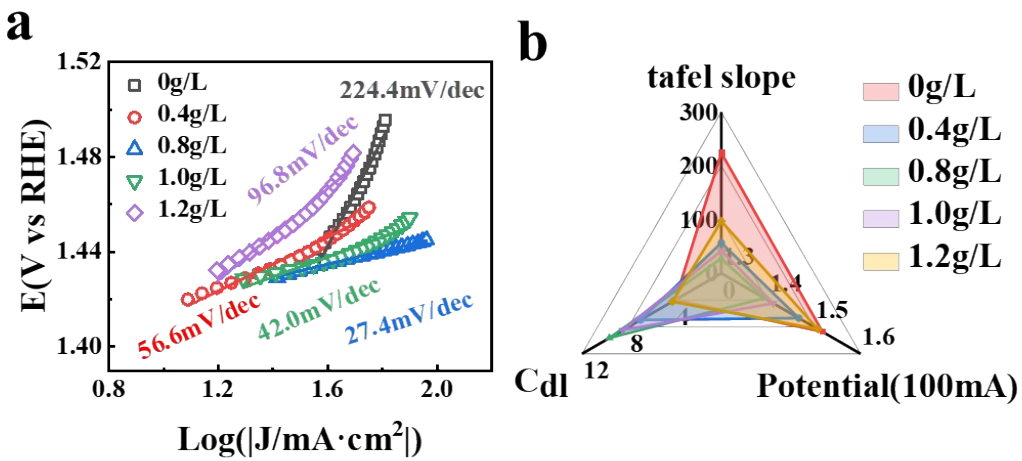

Figure S5 The influence of different K_2TaF_7 concentration on HMFOR performance of Ni-Ta-S-O

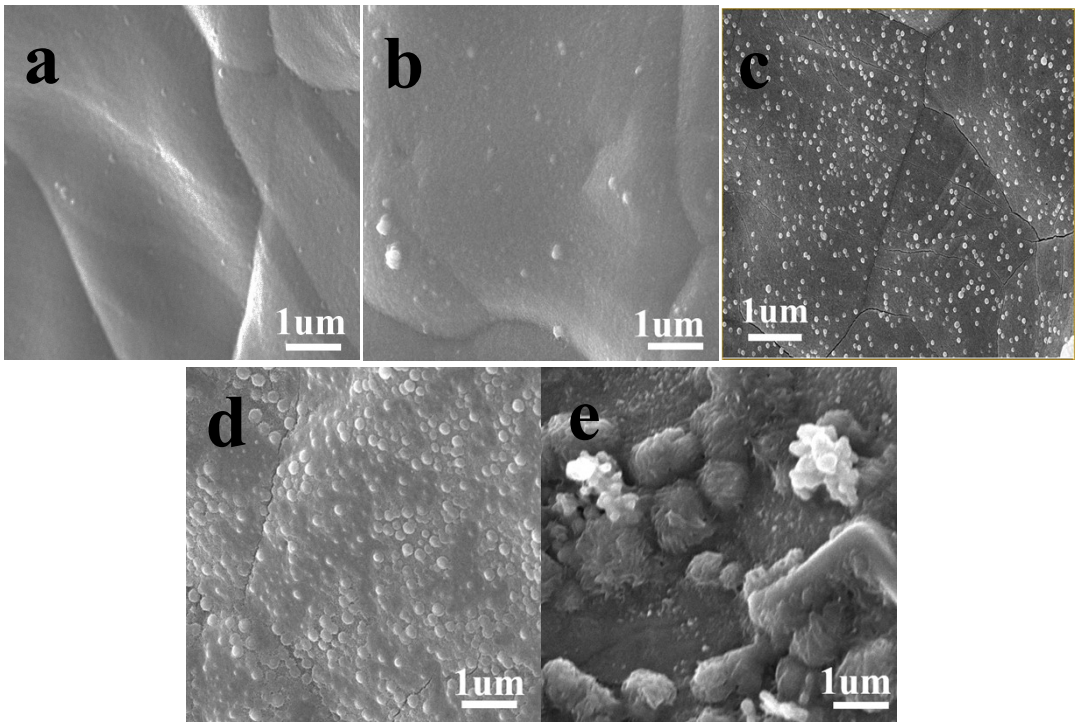

Figure S6 The influence of different K_2TaF_7 concentration on microstructure performance of Ni-Ta-S-O (a) 0 g/L (b) 0.4 g/L (c) 0.8g/L (d) 1.0 g/L (e) 1.2 g/L

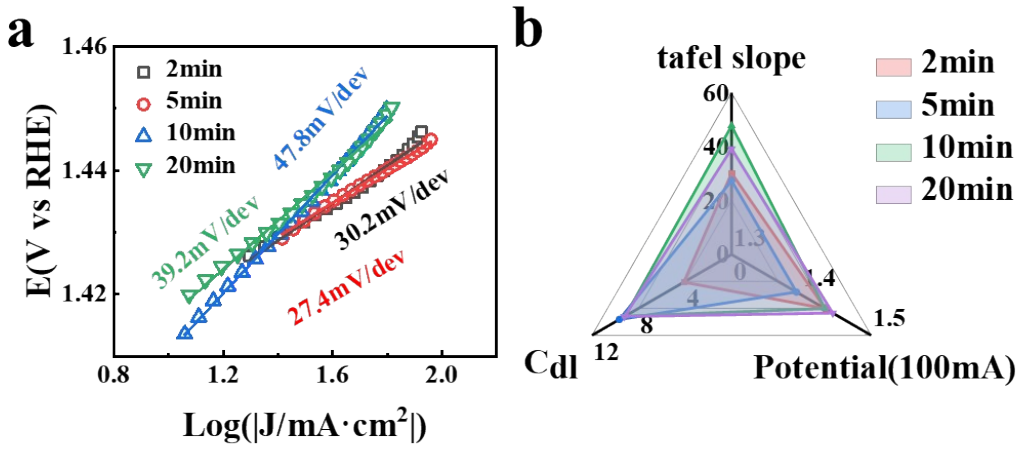

Figure S7 The influence of different reaction time on HMFOR performance of Ni-Ta-S-O

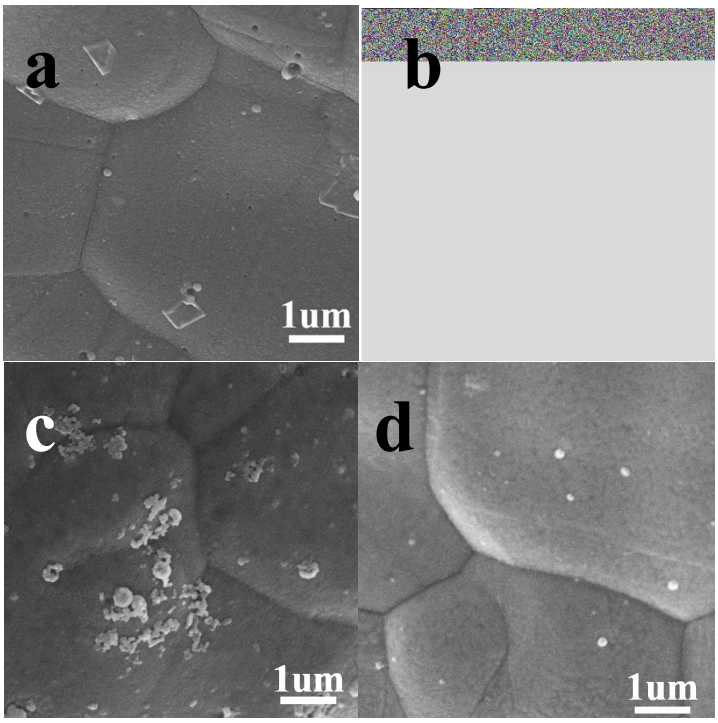

Figure S8 The influence of different reaction time on microstructure performance of Ni-Ta-S-O (a) 2min (b) 5min (c) 10min (d) 20min

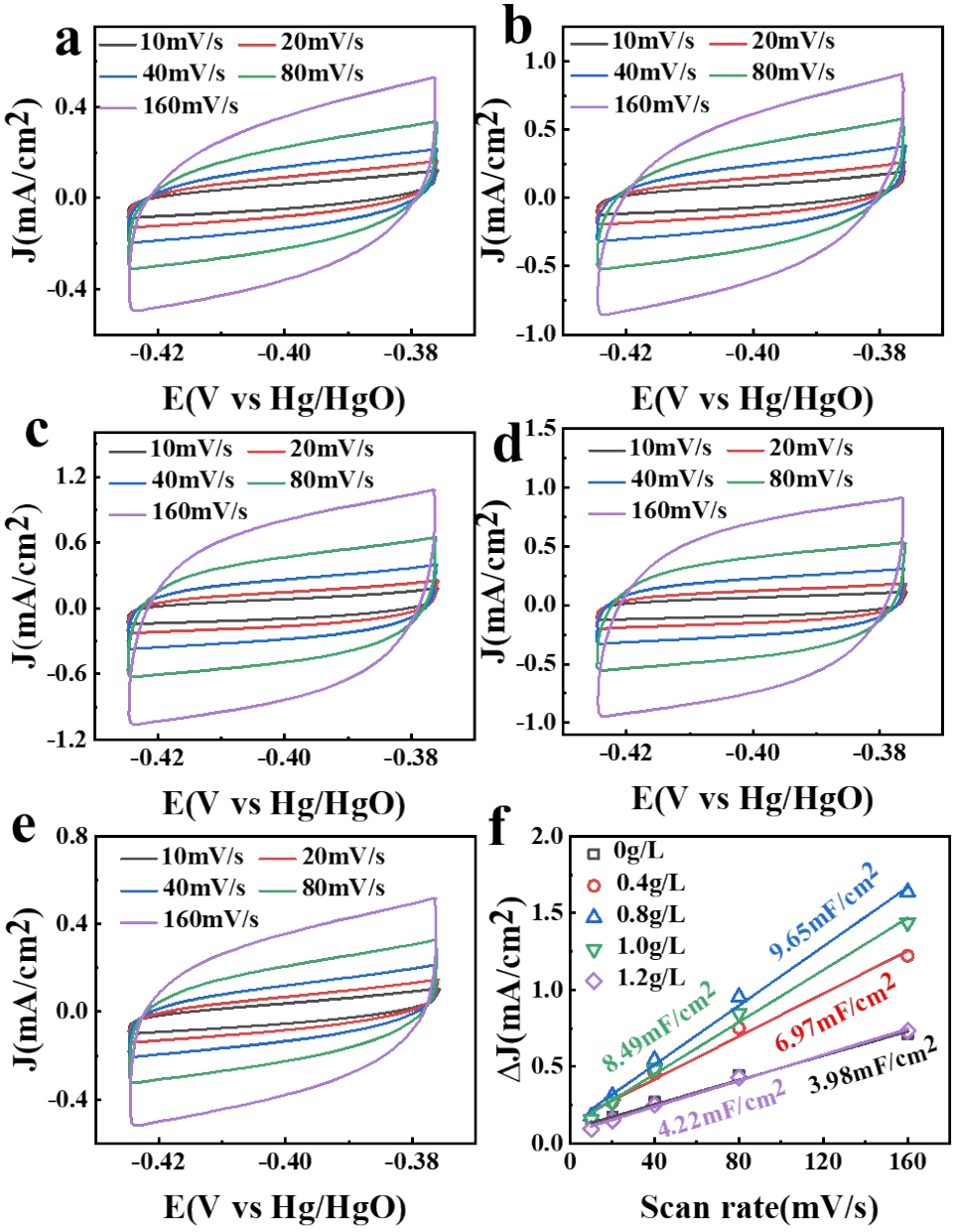

Figure S9 The influence of different K_2TaF_7 concentration on CV performance of Ni-Ta-S-O. The CV figure of the (a) 0 g/L (b) 0.4 g/L (c) 0.8g/L (d) 1.0 g/L (e) 1.2 g/L (f) The capacitive current difference at different scan rates at -0.4V (vs Hg/HgO).

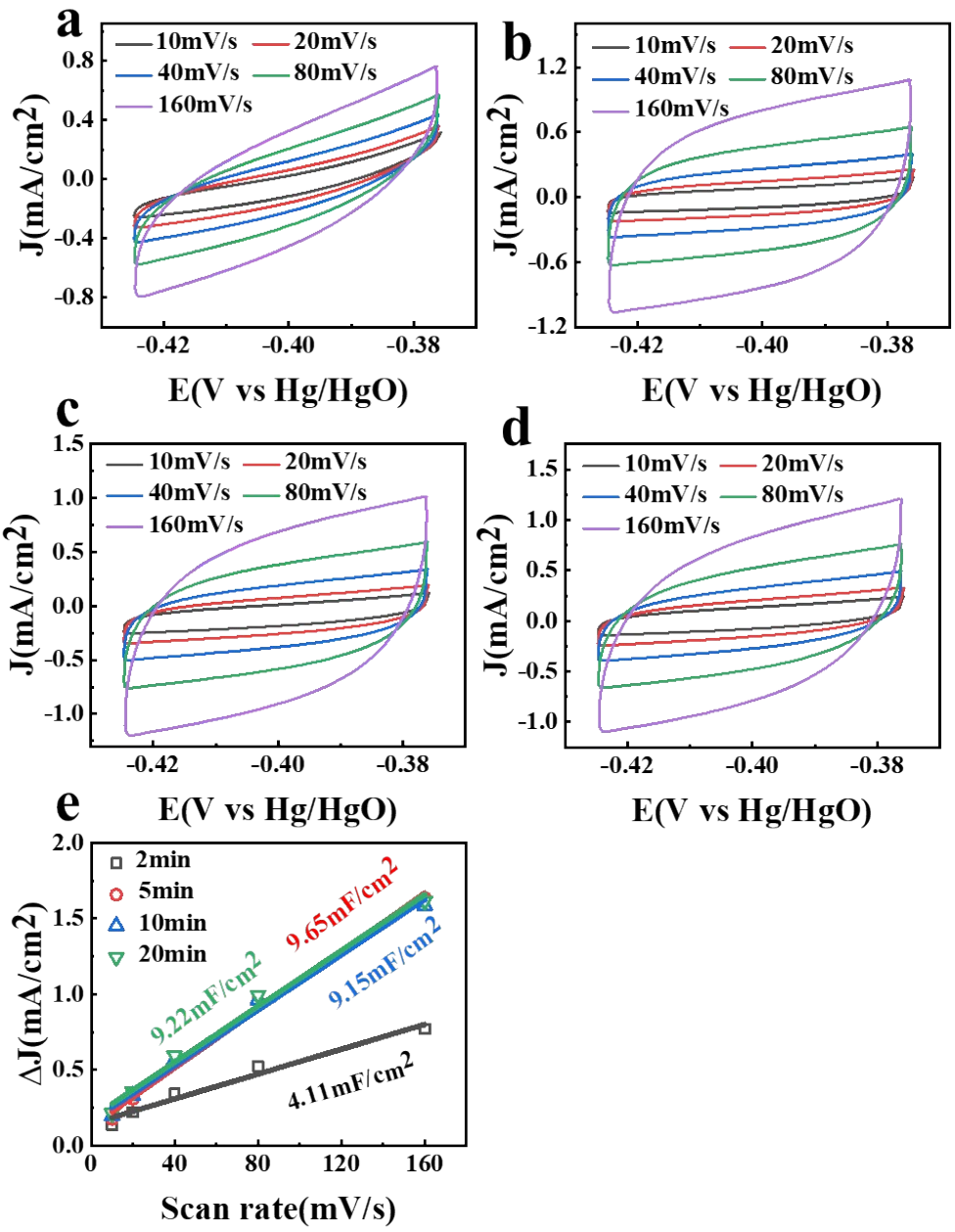

Figure S10 The influence of different reaction time on CV performance of Ni-Ta-S-O. The CV figure of the (a) 2min (b) 5min (c) 10min (d) 20min (e) The capacitive current difference at different scan rates at -0.4V(vs Hg/HgO).

Table S2 Comparison of electrochemical polarization resistance R_p value of different electrolyte under 0.55V(vs Hg/HgO) for Ni-Ta-S-O catalyst

electrolyte	$R_p(\Omega \cdot cm^2)$
KOH	38
KOH+HMF	1.38
KOH+NaCl+HMF	0.85

Table S3 Comparison of NO_2RR performance to previously reported electrocatalysts

FE(%)	E(V vs RHE)	NH_3 yield ($\mu mol/h \cdot cm^2$)	catalyst	ref
70	-0.2	89.6	**Zn_1/MnO_2**	10
76	-0.3	115.4	**In_1Cu**	11
91	-0.2	30	**Cu_2O nanocube**	12
75	-0.2	33.3	**Ni_1Ru**	13
79.8	-0.5	110.2	**L-Pd**	14
63.5	-0.4	45.0	**α-CoS_2**	15
72	-0.4	79.2	**Co_1Ru**	16
69.5	-0.2	31.5	**$CuRh_1$**	17
80.7	-0.4	73.47	**Au@CC-SDS**	18
79.0	-0.2	272.8	**CuFe-P**	19
90.2	-0.2	133.0	**CoP nanorray**	20
82	-0.2	64.7	**Ag@TiO_2**	21
85	-0.3	174.0	**Cu@TiO_2**	22
84	-0.2	59.8	**NiS_2@TiO_2**	23
97.0	-0.19	301.56①	**Ni-S-Ta-O**	This work
95.1	-0.19	3029.63②	**Ni-S-Ta-O**	This work
89.7	-0.20	278.86③	**Ni-S-Ta-O**	This work

Note:①1M KOH+1M KNO_2, without light;②1M KOH+1M KNO_2, with light;③1M KOH+1M KNO_2+0.6M NaCl, without light

Table S4 Comparison of HMFOR performance to previously reported electrocatalysts

tafel slope(mV/dec)	potential(100mA/cm2)	catalyst	ref
49.7	1.64	**S-NiFe LDH**	1
48.3	1.44	**Ni_3P-Cu_3P**	2
55	1.42	**$CoSe_2$/NiSe-$CoSe_2$**	3
78.11	1.48	**NiFeCe LDH**	4
38	1.41	**RuZn-NiFeS LDH**	5
88.0	1.35	**Ni-HITP/PW_{12}**	6
41.82	1.43	**NiFeMnB**	7
38	1.42	**V_O-$NiCo(OH)_2$**	8
64.8	1.52	**$Cu_{1/8}$-NiO**	9
19.0	1.40①	**Ni-S-Ta-O**	This work
27.4	1.39②	**Ni-S-Ta-O**	This work
26.5	1.37②	**Ni-S-Ta-O**	This work

Note:①1M KOH+0.1M HMF, without light;②1M KOH+0.6M NaCl+0.1M HMF, without light;③1M KOH+0.6M NaCl+0.1M HMF, with light

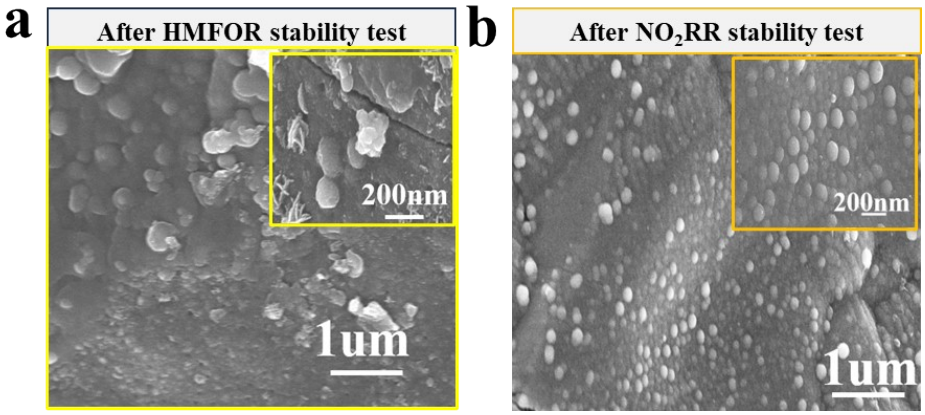

Fig. S11 SEM image of Ni-Ta-S-O catalyst after HMFOR(b) stability test and after NO2RR(c) stability test

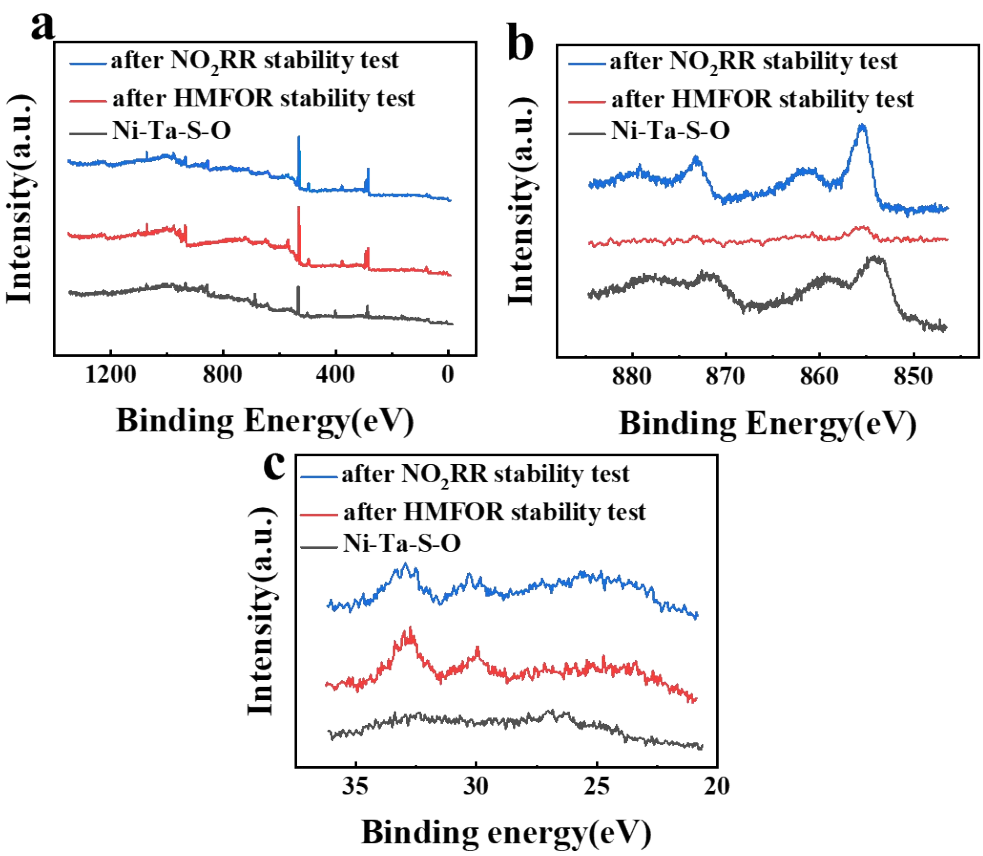

Fig. S12 XPS full spectrum(a), Ni2p spectrum(b) and Ta 4f spectrum(c) of Ni-Ta-S-O/CF, and Ni-Ta-S-O/CF after HMFOR and after NO2RR stability tests.

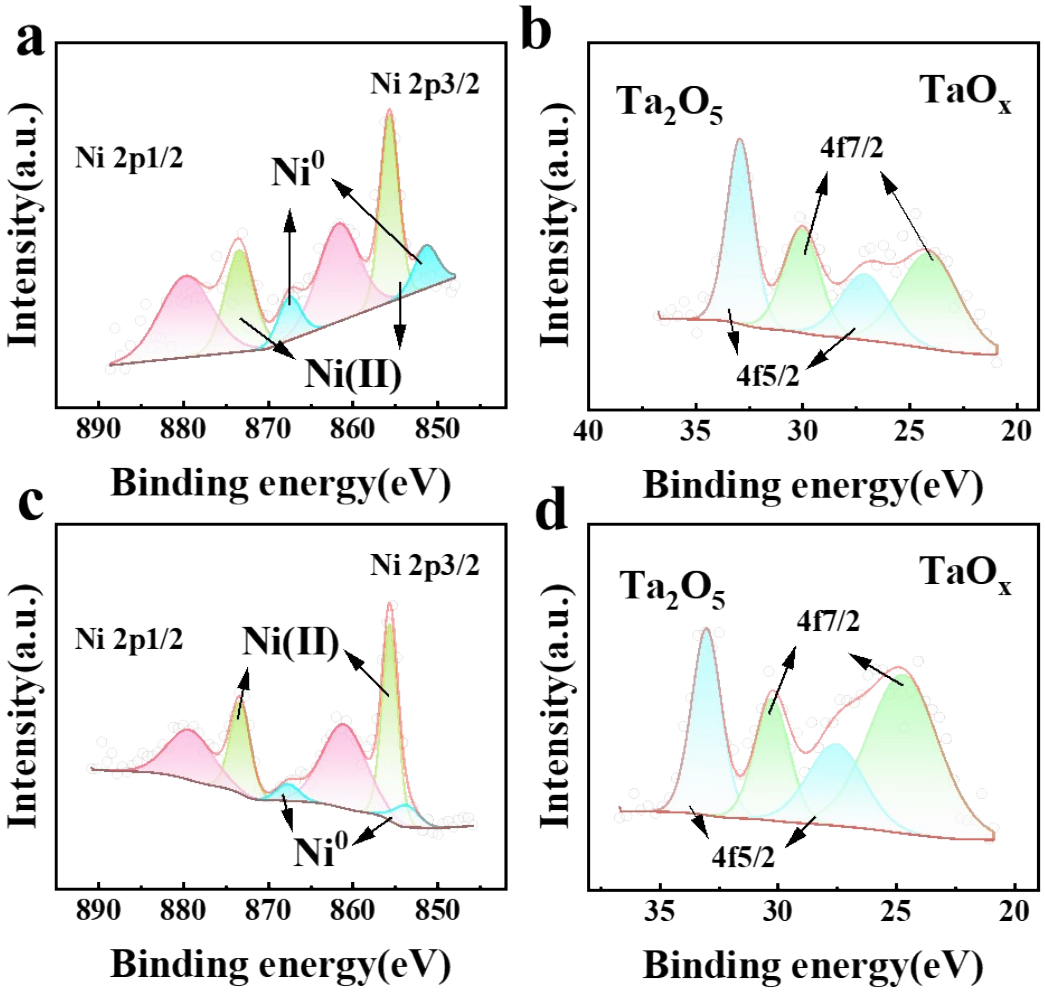

Fig. S13 The XPS fine spectra of Ni and Ta element of Ni-Ta-S-O catalytic layer after HMFOR and NO2RR stability test. (a) The XPS fine spectra of Ni element of Ni-Ta-S-O catalytic layer after HMFOR stability test (b) The XPS fine spectra of Ta element of Ni-Ta-S-O catalytic layer after HMFOR stability test. (c) The XPS fine spectra of Ni element of Ni-Ta-S-O catalytic layer after NO2RR stability test. (d) The XPS fine spectra of Ta element of Ni-Ta-S-O catalytic layer after NO2RR stability test.

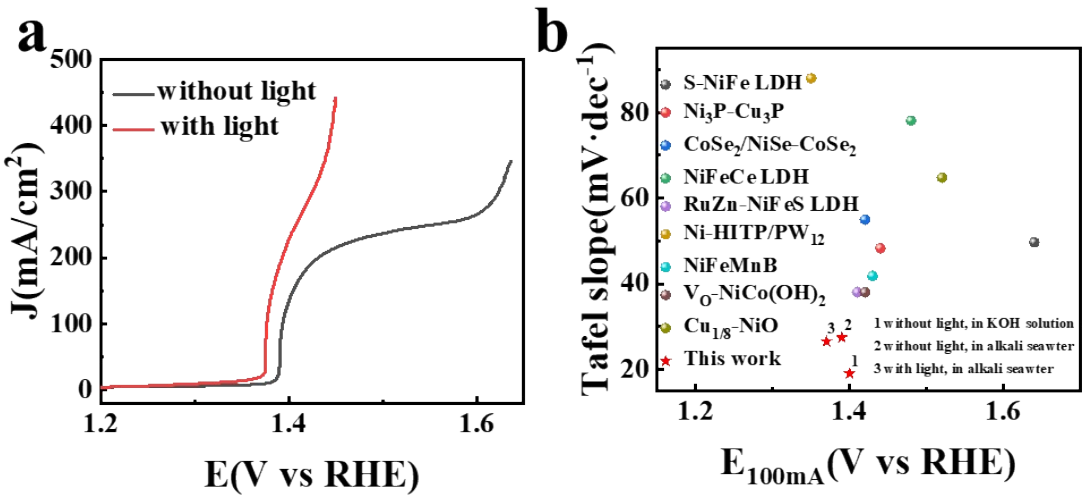

Fig. S14 LSV performance of Ni-Ta-S-O catalyst under no light and light condition and the comparison of HMFOR performance based on as-reported HMF catalysts

Table S5 Comparison of nitrate/nitrite to ammonia electrolytic cells performance based on previously reported dual-function electrocatalysts

catalyst	Apply	E(V)	ref
Cu_2NCN	NO_3RR/GlyOR	1.51V@100mA/cm^2	24
	NO_3RR/OER	1.78V@100mA/cm^2	
Ov-$Co(OH)_2$/Cu	NO_2RR/GluOR	1.68V@100mA/cm^2	25
	NO_2RR/OER	2.25V@100mA/cm^2	
CuO/Co_3O_4	NO_3RR/HMFOR	1.78V@50mA/cm^2	26
Co_3O_4/NF	NO_2RR/OER	2.5V@50mA/cm^2	27
	NO_2RR/SOR	1.7V@75mA/cm^2	
β-$Co(OH)_2$/$Cu_2(OH)_2Cl$	NO_2RR/GlyOR	1.82V@100mA/cm^2	28
Ni-S-Ta-O	NO_2RR/OER	1.94V@100mA/$cm^2$①	This work
		1.40V@100mA/$cm^2$②	
Ni-S-Ta-O	NO_2RR/HMFOR	1.61V@100mA/$cm^2$①	This work
		1.22V@100mA/$cm^2$②	

Note: ①without light;②with light

Table S6 Comparison of electrochemical stability of previously reported dual-function electrocatalysts for nitrate/nitrite to ammonia electrolytic cells

catalyst	Apply	time(h)	Current/voltage retention rate(%)	ref
Cu_2NCN	NO_3RR/GlyOR	105	82.4	24
Ov-$Co(OH)_2$/Cu	NO_2RR/GluOR	48	76.8	25
CuO/Co_3O_4	NO_3RR/HMFOR	--	--	26
Co_3O_4/NF	NO_2RR/SOR	120	87.7	27
β-$Co(OH)_2$/$Cu_2(OH)_2Cl$	NO_2RR/GlyOR	24	91.2	28
Cu/NiFe LDH	NO_3RR/OER	12	95.4	30
NiCoFeV-S	NO_3RR/OER	25	97.1	31
NiP_x/CoS_x	NO_3RR/SOR	20	81.3	32
Ni-S-Ta-O	NO_2RR/HMFOR	100	86.05	This work

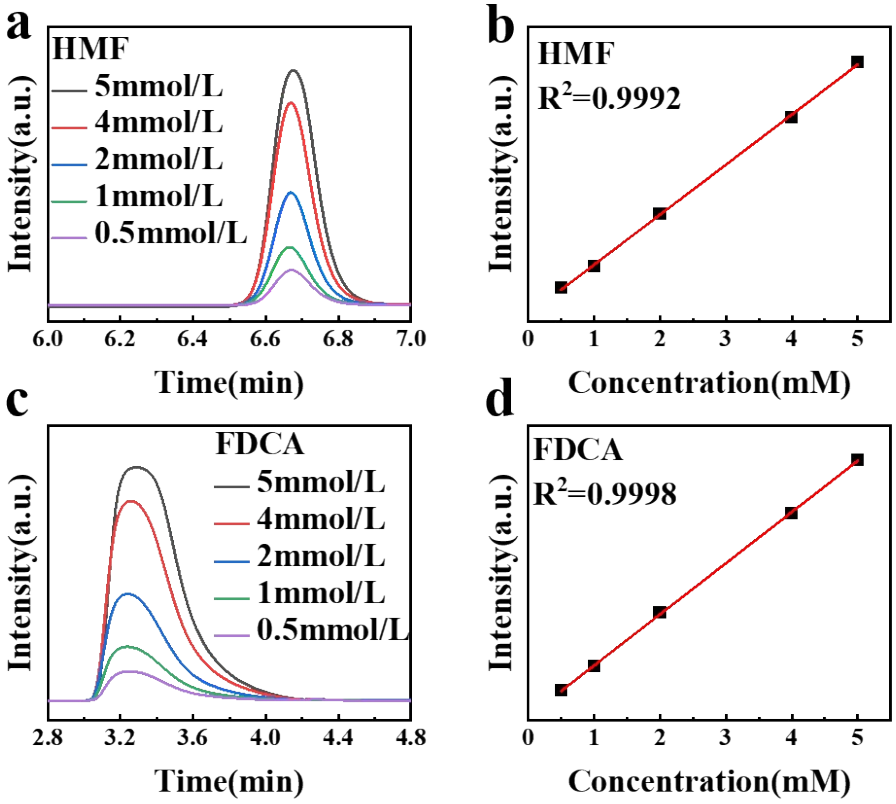

Figure S15 The peak position and standard curve of HMF (a, b) and FDCA (c, d).

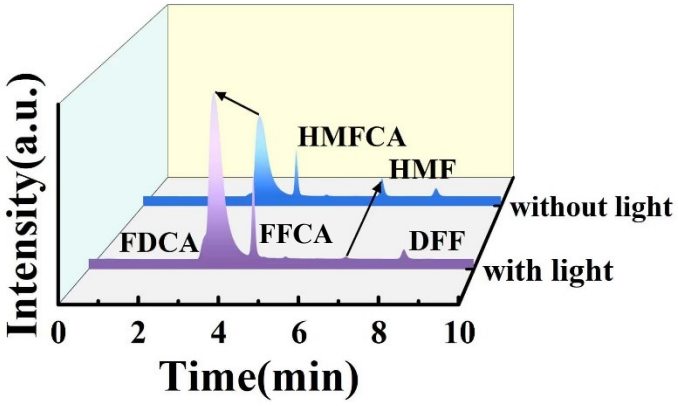

Figure S16 Comparison of FDCA product yield under pure electric field and light-electric field conditions

Table S7 Comparison of FDCA product yield under pure electric and light-electric conditions

	without light(%)	**with light(%)**
HMF conversion	91.9	99.3
FDCA yield	39.1	78.9
F.E.(FDCA)	64.4	84.4
Selectivity(FDCA)	42.5	79.5

REFERENCES

1 J. Zhang, Y. Yang, G. Ding, Z. Wang, P. Wang, C. Li, and G. Liao, *Chem. Eng. J.*, 2025, **505**, 159165.

2 J. Fu, G. Yang, Y. Jiao, C. Tian, H. Yan, and H. Fu, *Nano Energy*, 2024, **127**, 109727.

3 S. Liu, W. Cai, M. Jin, T. Zhang, Z. Zhang, Q. Liu, X. Liu, X. Zhang, and F. Wang, *Adv. Funct. Mater.*, 2025, **35**, 2421447.

4 Y. Zhang, G. Hai, Z. Huang, Z. Liu, X. Huang, and G. Wang, *Adv. Energy Mater.*, 2024, **14**, 2401449.

5 H. Xu, L. Lu, Z. Yu, X. Lu, Y. Duan, C. Si, and X. Li, *Appl. Catal. B*, 2025, **375**, 125439.

6 T. Bao, Y. Wu, C. Tang, Y. Xi, Y. Zou, P. Shan, C. Zhang, W. Drożd, A. R. Stefankiewicz, P. Yuan, C. Yu, and C. Liu, *Adv. Mater.*, 2025, **37**, 2500399.

7 L. Shi, W. Cai, F. Zhang, S. Li, X. Liu, Y. Liu, P. Ren, B. Li, S. Liu, and B. Liu, *Angew. Chem., Int. Ed.*, 2025, **64**, e202424345.

8 D. Xie, J. Chen, J. Hou, F. Yang, R. Feng, C. Cao, and Z. Xie, *J. Energy Chem.*, 2025, **108**, 558–566.

9 K. Guo, C. Du, Y. Tu, and Z. Ren, *Adv. Funct. Mater.*, 2025, 2505043.

10 Y. Wan, Y. Zhang, N. Zhang, Z. Zhang, and K. Chu, *Chem. Eng. J.*, 2024, **481**, 148734.

11 F. Wang, S. Shang, Z. Sun, X. Yang, and K. Chu, *Chem. Eng. J.*, 2024, **489**, 151410.

12 L. Bai, F. Franco, J. Timoshenko, C. Rettenmaier, F. Scholten, H. S. Jeon, A. Yoon, M. Rüscher, A. Herzog, F. T. Haase, S. Kühl, S. W. Chee, A. Bergmann, and B. Roldan Cuenya, *J. Am. Chem. Soc.*, 2024, **146**, 9665–9678.

13 F. Wang, H. Zhao, G. Zhang, H. Zhang, X. Han, and K. Chu, *Adv. Funct. Mater.*, 2024, **34**, 2308072.

14 W. Qu, T. Wu, J. Wang, X. Liu, Y. Tian, and K. Chu, *New J. Chem.*, 2024, **48**, 4346–4350.
15 Y. Qu, Y. Guo, and K. Chu, *Inorg. Chem.*, 2024, **63**, 78–83.
16 F. Wang, J. Xiang, G. Zhang, K. Chen, and K. Chu, *Nano Res.*, 2024, **17**, 3660–3666.
17 J. Xiang, C. Qiang, S. Shang, K. Chen, C. Kang, and K. Chu, *Adv. Funct. Mater.*, 2024, **34**, 2401941.
18 W. Zhang, T. Wang, X. Xing, H. Yin, J. Li, W. Xiong, and H. Li, *ACS Sustainable Chem. Eng.*, 2024, **12**, 10313–10324.
19 G. Wang, C. Wang, X. Tian, Q. Li, S. Liu, X. Zhao, G. I. N. Waterhouse, X. Zhao, X. Lv, and J. Xu, *Small*, 2024, **20**, 2311439.
20 G. Wen, J. Liang, Q. Liu, T. Li, X. An, F. Zhang, A. A. Alshehri, K. A. Alzahrani, Y. Luo, Q. Kong, and X. Sun, *Nano Res.*, 2022, **15**, 972–977.
21 Q. Liu, G. Wen, D. Zhao, L. Xie, S. Sun, L. Zhang, Y. Luo, A. A. Alshehri, M. S. Hamdy, Q. Kong, and X. Sun, *J. Colloid Interface Sci.*, 2022, **623**, 513–519.
22 L. Ouyang, X. Fan, Z. Li, X. He, S. Sun, Z. Cai, Y. Luo, D. Zheng, B. Ying, J. Zhang, A. A. Alshehri, Y. Wang, K. Ma, and X. Sun, *Chem. Commun.*, 2023, **59**, 1625–1628.
23 X. He, L. Hu, L. Xie, Z. Li, J. Chen, X. Li, J. Li, L. Zhang, X. Fang, D. Zheng, S. Sun, J. Zhang, A. A. Alshehri, Y. Luo, Q. Liu, Y. Wang, and X. Sun, *J. Colloid Interface Sci.*, 2023, **634**, 86–92.
24 J. Wang, H. T. D. Bui, H. Hu, S. Kong, X. Wang, H. Zhu, J. Ma, J. Xu, Y. Liu, L. Liu, W. Chen, H. Bi, M. Yang, F. Huang, T. Brinck, and J. Wang, *Adv. Mater.*, 2025, **37**, 2418451.
25 W. Mei, C. Chang, Z. Li, X. Wang, Y. Qie, Q. Liu, R. C. Davis, Z. Wu, Y. Yue, C. Yang, S. Li, D. Han, Q. Yang, Z. Feng, and Z. Weng, *Adv. Mater.*, 2025, 2507363.
26 L. Zhang, P. Jin, Z. Wu, B. Zhou, J. Jiang, A. Deng, Q. Li, T. Hussain, Y. Zhang, H. Liu, and S. Wang, *Energy Environ. Mater.*, 2024, **7**, e12725.
27 C. Zhang, X. Wang, J. Jiang, J. Zhang, A. Liu, and L. Ai, *Appl. Catal. B*, 2025, **365**, 124991.
28 M. Wang, P. Chen, H. Wang, and Y. Zhao, *J. Energy Chem.*, 2025, **104**, 185–193.
29 X. Jiang, W. Li, Y. Liu, L. Zhao, Z. Chen, L. Zhang, Y. Zhang, and S. Yun, *Susmat* 2023, **3**, 21-43.
30 F. Du, J. Yao, H. Luo, Y. Chen, Y. Qin, Y. Du, Y. Wang, W. Hou, M. Shuai, and C. Guo, *Green Chem.,* 2024, **26**(2), 895-903.
31 Y. Lei, L. Zhang, X. Wang, D. Wang, Y. Zhao, B. Zhang, N. Zhang, and H. Shang, *Chem. Sci.*, 2025, **16**(39), 18298-18308.
32 B. Tang, K. Jiang, W. Yin, W. Xing, J. Zhang, S. Pi, J. Liang, L. Tang, and W. Tang, *Small,* 2025, **21**(45), e08173.